Systems/Circuits

State-Dependent Contribution of the Hyperpolarization-Activated Na^+/K^+ and Persistent Na^+ Currents to Respiratory Rhythmogenesis *In Vivo*

Gaspard Montandon and Richard L. Horner
Departments of Medicine and Physiology, University of Toronto, Toronto, Ontario M5S 1A8, Canada

How rhythms are generated by neuronal networks is fundamental to understand rhythmic behaviors such as respiration, locomotion, and mastication. Respiratory rhythm is generated by the preBötzinger complex (preBötC), an anatomically and functionally discrete population of brainstem neurons, central and necessary for respiratory rhythm. In specific *in vitro* conditions, preBötC neurons depend on voltage-dependent inward currents to generate respiratory rhythm. In the mature and intact organism, where preBötC neurons are deeply embedded in the respiratory network, the contribution of ionic currents to respiratory rhythm is unclear. We propose that a set of ionic currents plays a key role in generating respiratory rhythm in the mature organism *in vivo*. By microperfusing ionic current blockers into the preBötC of adult rats, we identify the hyperpolarization-activated cation current as a critical component of the mechanism promoting respiratory rhythm, and that this current, in combination with the persistent sodium current, is essential to respiratory rhythm *in vivo*. Importantly, both currents contribute to rhythmic activity in states of anesthesia, quiet wakefulness, and sleep, but not when the organism is engaged in active behaviors. These data show that a set of ionic currents at the preBötC imparts the network with rhythmicity in reduced states of arousal, although the network can override their contribution to adjust its activity for nonrhythmic behaviors in active wakefulness.

Introduction

Neuronal networks mediate essential rhythmic behaviors, such as locomotion, mastication, and breathing (Feldman and Del Negro, 2006; Zhong et al., 2007). Breathing emerges from the respiratory rhythmic network which expresses a regular and simple rhythmic motor activity, yet orchestrated by a complex network of brainstem neurons. At its core is the preBötzinger complex (preBötC), an anatomically and functionally discrete population of brainstem neurons, central and necessary for respiratory rhythm (Smith et al., 1991; Gray et al., 2001). In the preBötC, voltage-dependent ionic currents, such as the persistent sodium current I_{NaP} or the calcium-activated cation current, play key roles in mediating respiratory rhythm (Pena et al., 2004), and their roles are apparent in specific *in vitro* (Pena et al., 2004; Paton et al., 2006) and *in vivo* conditions (Pena and Aguileta, 2007; St-John et al., 2007). I_{NaP} often interacts with other inward currents to promote rhythm (Pape, 1996). The hyperpolarization-activated cation current (I_h), for instance, mediates rhythms in various networks when combined with I_{NaP} (Biel et al., 2009). I_h was detected in preBötC neurons (Mironov et al., 2000) but blockade of I_h current in immature rodents studied *in vitro* elicits conflicting results as it had either no effect on rhythm (Mironov et al., 2000) or increased respiratory rhythm (Thoby-Brisson et al., 2000). I_h and I_{NaP} expressions, however, substantially increase as the organism matures (Bayliss et al., 1994; Cho et al., 2011), therefore limiting our understanding of their contributions in the mature network. Here, we aim to understand the role of I_h and I_{NaP} in the generation of respiratory rhythm in the intact and mature organism *in vivo*.

Respiratory rhythm is a robust autonomic motor behavior that is continuously generated to maintain homeostasis. In reduced states of brain arousal, such as sleep or anesthesia, respiratory rhythm is generated by mechanisms within the brainstem respiratory network, that do not require voluntary activation of respiratory muscles. The network has, however, the capacity to override automatic rhythm to coordinate its activity with behaviors, such as grooming or feeding. In fact, respiratory rhythm is typically erratic when an organism is behaviorally active and closely follows behaviors, but it becomes more regular when the organism progresses from quiet wakefulness to deep sleep (Phillipson and Bowes, 1986). PreBötC neurons are likely involved in these state-dependent changes because their destruction or inhibition induces unstable rhythm and respiratory depression especially in states of reduced brain arousal (McKay et al., 2005; Montandon et al., 2011). Here, we propose that the robust rhythmicity observed in reduced arousal states is dependent on ionic currents, but that this mechanism is overridden

Received Oct. 26, 2012; revised April 4, 2013; accepted April 8, 2013.

Author contributions: G.M. and R.L.H. designed research; G.M. performed research; G.M. analyzed data; G.M. and R.L.H. wrote the paper.

This work was supported by the Parker B. Francis Fellowship (G.M.), the Ontario Ministry of Research and Innovation Fellowship (G.M.), the Canadian Institutes for Health Research (R.L.H.), and the Tier 1 Canada Research in Sleep and Respiratory Neurobiology (R.L.H.).

The authors declare no competing financial interests.

Correspondence should be addressed to either Gaspard Montandon or Richard L. Horner, University of Toronto, 1 King's College Circle, Toronto, ON M5S 1A8, Canada, E-mail: gaspard.montandon@utoronto.ca or richard.horner@utoronto.ca.

DOI:10.1523/JNEUROSCI.5066-12.2013

 0270-6474/13/338716-13$15.00/0

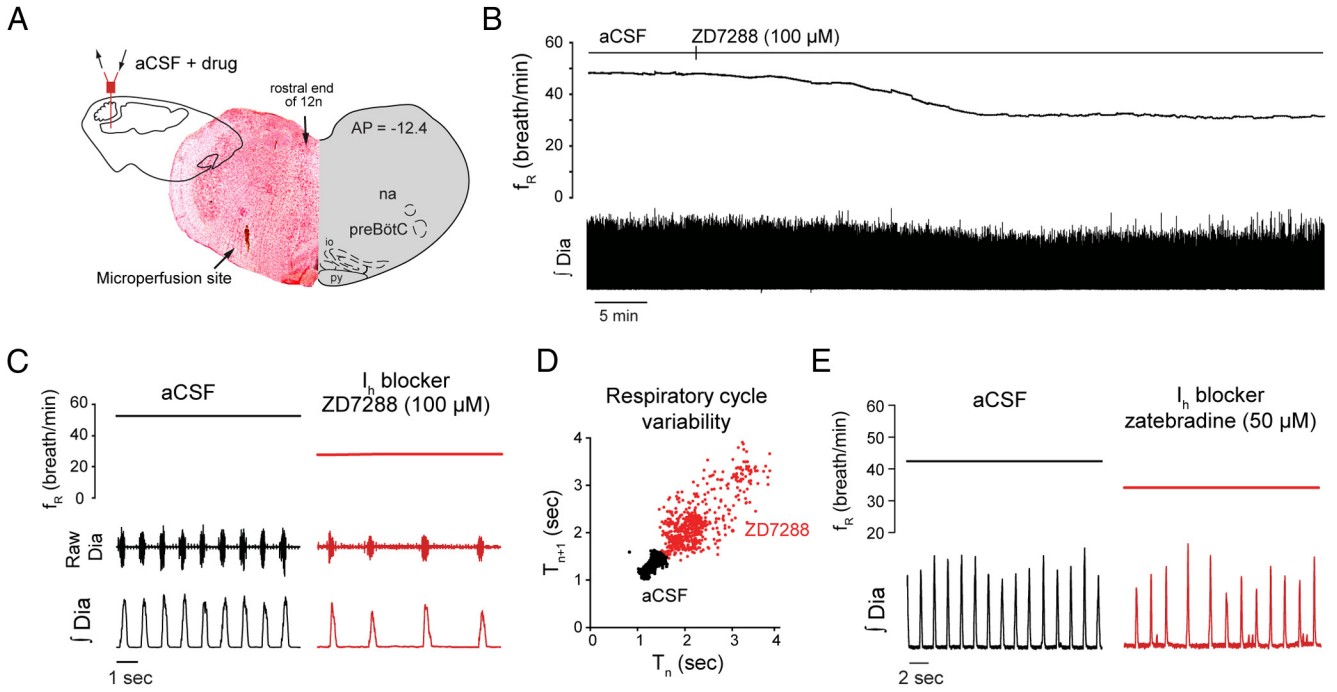

Figure 1. I_h at the preBötC modulates respiratory rhythm. ***A***, ***B***, Unilateral application of ZD7288 decreased respiratory rhythm in the anesthetized adult rat *in vivo*. Histology shows that ZD7288 was microperfused in the region of the preBötC (arrow shows microperfusion site). ***C***, Unilateral microperfusion of ZD7288 (100 μM) to the preBötC reduced respiratory frequency ($n = 5$) without significantly affecting diaphragm amplitude. ***D***, Cycle-by-cycle variability with Poincare plots revealed that ZD7288 increased short-term variability. ***E***, Unilateral microperfusion of zatebradine (50 μM) into the preBötC reduced respiratory frequency and diaphragm amplitude ($n = 3$). f_R, Respiratory frequency; Raw Dia, diaphragm electromyogram; ∫Dia, rectified and moving time averaged diaphragm activity; T_n, respiratory period; T_{n+1}, respiratory period of the following respiratory cycle; na, nucleus ambiguus; 12n, hypoglossal nucleus; io, inferior olive; py, pyramidal tract.

when the organism is engaged in active behaviors. By applying agents to the preBötC with anatomical and functional specificity (Montandon et al., 2011), we show that I_h or I_{NaP} blockers reduced respiratory rhythm and abolished breathing only when applied in combination. Importantly, we demonstrate that these blockers also decreased respiratory rhythm in the freely behaving organism, with this effect only present in quiet wakefulness and sleep, but not in active wakefulness. In summary, I_h and I_{NaP} contribute to respiratory rhythm in states of reduced brain arousal in the intact rodent, although the respiratory network can override their contributions to coordinate its activity with non-respiratory behaviors in active wakefulness.

Materials and Methods

All procedures were performed in accordance with the recommendations of the Canadian Council on Animal Care, and were approved by the University of Toronto Animal Care Committee.

Anesthetized preparations. To determine the contribution of I_h and I_{NaP} at the preBötC on respiratory activities, we used reverse-microdialysis to microperfuse selected agents into the preBötC of anesthetized adult male Wistar rats ($n = 34$) weighing between 280 and 320 g. The experimental procedures were described previously (Montandon et al., 2011). Briefly, we recorded diaphragm and genioglossus muscle activities in isoflurane-anesthetized (2–2.5%), tracheotomized and spontaneously breathing (50% oxygen–gas mixture, balance nitrogen) adult rats while microperfusing agents into the preBötC. Electrical signals were amplified, filtered, and averaged with a moving time window (100 ms). Raw and averaged signals were recorded on a computer with Spike 2 software (v 6 and Micro-1401, Cambridge Electronic Design). Using a dorsal approach, a microdialysis probe (CX-I-12–01, diameter 200 μm, length of diffusing membrane 1 mm, Eicom) was inserted into the brainstem 2.0 mm dorsal to the preBötC using a stereotaxic frame and micromanipulator with a resolution of 50 μm (ASI Instruments). The microdialysis probe was continuously perfused at 3 μl/min with freshly made artificial CSF (aCSF). The composition of the aCSF was (in mM): 125 NaCl, 3 KCl, 1 KH_2PO_4, 2 $CaCl_2$, 1 $MgSO_4$, 25 $NaHCO_3$, and 30 glucose. The pH was adjusted at 7.4 by bubbling CO_2 in the aCSF. The probe was initially placed 12.2 mm posterior, 2 mm lateral, and 8.5 mm ventral to bregma, was then progressively lowered into the brainstem while recording all physiological variables, and was left in place when genioglossus muscle activity decreased by ~30% which typically occurred with the probe ~10.5 mm ventral to bregma. We note that this response is a good initial marker of the appropriate depth of the probe before subsequent confirmation by postmortem histology (Montandon et al., 2011).

Baseline levels of the physiological variables were recorded for at least 30 min. Following this control period, the I_h blockers ZD7288 (100 μM) and zatebradine (50 μM; Tocris Bioscience), the I_{NaP} blocker riluzole (50 μM, riluzole hydrochloride; Tocris Bioscience), the voltage-gated sodium channel (Na_V) activator veratridine (100 nM; Tocris Bioscience), and the Na_V1 blocker ranolazine (100 μM, Tocris Bioscience) were added to the aCSF for microperfusion into the preBötC region. The responses to ZD7288 ($n = 9$), zatebradine ($n = 3$), riluzole ($n = 10$), veratridine ($n = 5$), and ranolazine ($n = 4$) were recorded for the next 60 min. For the riluzole experiments, riluzole microperfusion was then followed by washout with aCSF for 60 min. In a separate set of experiments, we also bilaterally microperfused either ZD7288 (100 μM) or a combination of 50 μm riluzole and 100 μm ZD7288 into both preBötCs to determine whether it would abolish respiratory activity altogether ($n = 3$). To evaluate the frequency-dependent effect of ZD7288 and riluzole, we correlated the percentage change in respiratory frequency with the initial (i.e., baseline) conditions. The initial baseline frequency varied between 30 and 50 breath/min due to the inherent variation between preparations due to the variable sensitivity to anesthetized agents and probe placement. To evaluate instantaneous variability of the cyclic period (T), we plotted T_{n+1} as a function of the preceding cycle T_n and calculated the index of cycle-by-cycle variability. This index is equivalent to the SD of the successive differences of cyclic periods. By comparing each cycle with its preceding cycle, this index excludes the variability due to slow degradation of rhythm over time.

Changes from aCSF in response to drug treatment were determined with one-way repeated-measure ANOVAs (drug application being the

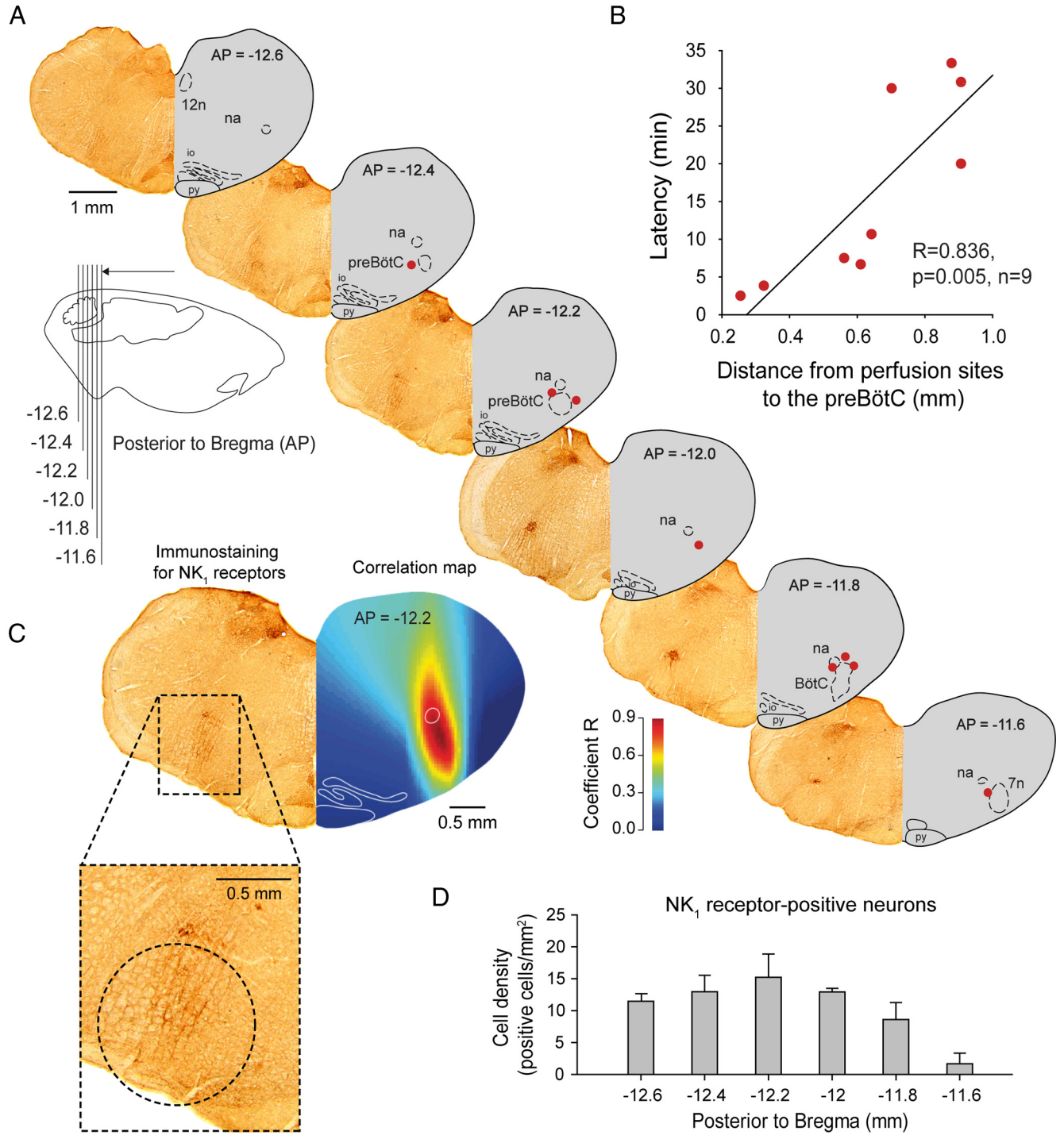

Figure 2. Sites of action of the I_h blocker ZD7288 and NK1R expression in the ventrolateral medulla. ***A***, Sections showing NK1R expression (left hemisection) and microperfusion sites (right hemisection, red circles) in the ventrolateral medulla 12.6–11.6 mm posterior to bregma. The perfusion sites were in the vicinity of the preBötC. Each perfusion site corresponds to one experiment with microperfusion in the preBötC region. ***B***, There was a significant correlation between the latencies for ZD7288 to depress frequency by 10% and the distances of the perfusion sites from the preBötC (coordinates AP = −12.2, ML = 2.3, DV = −10.4) in anesthetized rats, showing that perfusion of drugs close to the preBötC has a faster effect on frequency than perfusion away from it. ***C***, Correlation map shows that the neural site most sensitive to ZD7288 corresponds to NK1R expression. ***D***, Density of NK1R-expressing cells (see circle shown in ***C***) from 11.6 to 12.6 mm posterior to bregma. 7n, Facial nucleus. Values are shown as means ± SEM.

repeated factor) followed by Dunnet's *post hoc* tests for comparison with a single control (i.e., aCSF). $p < 0.05$ was considered statistically significant. Data are presented as means ± SEM.

Freely behaving preparations. To determine the effects of I_h and I_{NaP} blockade at the preBötC on respiratory activity across sleep–wake states, we perfused riluzole (50 μM), ZD7288 (100 μM), or a combination of ZD7288 (100 μM) and riluzole (50 μM) bilaterally into both preBötCs of freely behaving male adult Wistar rats ($n = 13$). One week before the experiments, sterile surgery was performed under isoflurane anesthesia to implant the rats with electroencephalogram (EEG) and postural (neck) muscle electrodes to identify sleep–wake states, and diaphragm and genioglossus muscle electrodes for respiratory muscle recordings as previously described (Montandon et al., 2011). Two microdialysis guide cannulas (AG-8, Eicom) were positioned 5.0 mm above the preBötC by

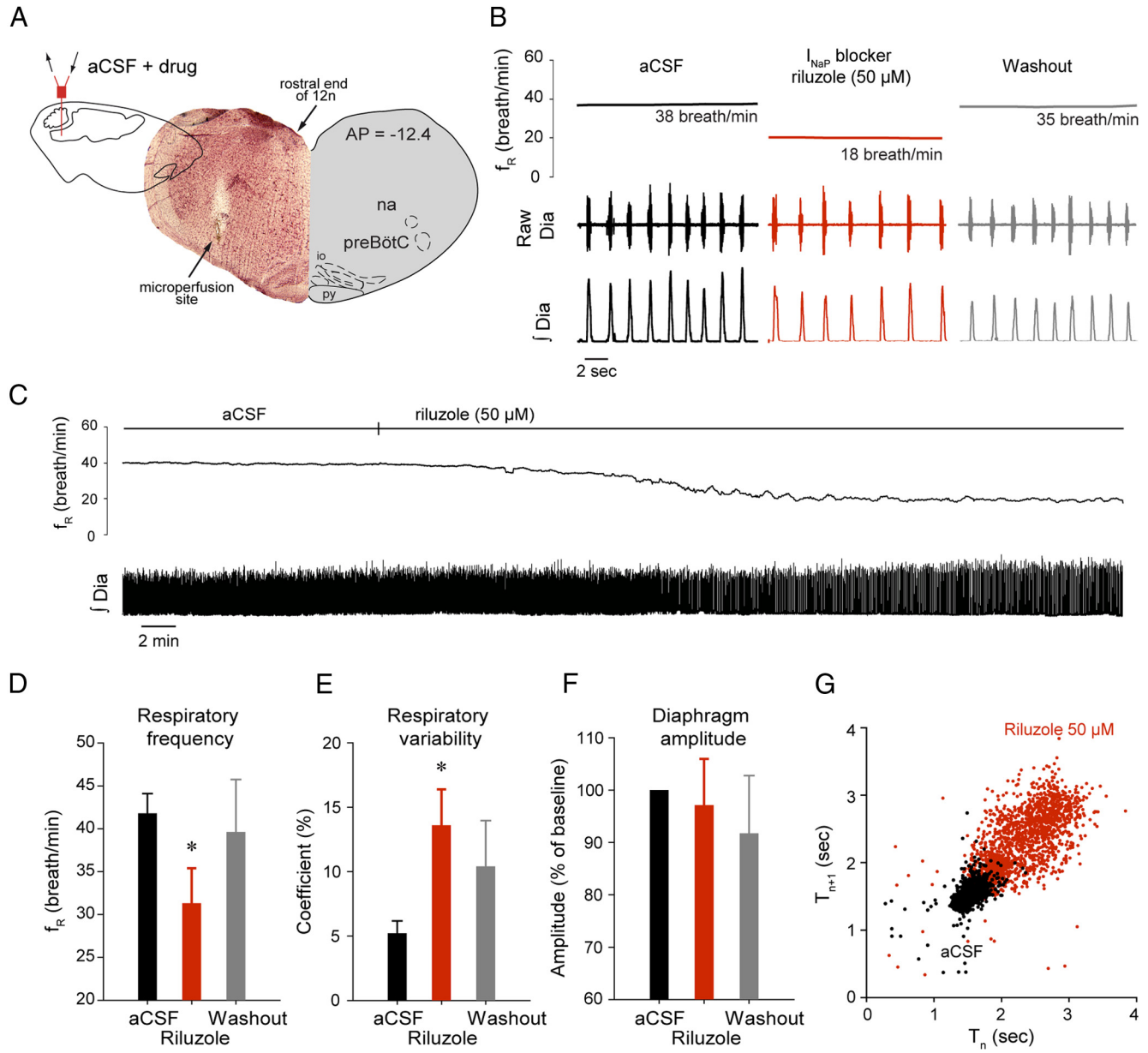

Figure 3. I_{NaP} at the preBötC modulates respiratory rhythm. ***A–C***, Unilateral microperfusion of the I_{NaP} blocker riluzole (50 μM) into the preBötC decreased respiratory rhythm ($n = 6$) in the anesthetized adult rat *in vivo* (arrow shows perfusion site). ***D–F***, Mean values showed that riluzole significantly reduced respiratory frequency, increased respiratory variability, without significantly affecting diaphragm amplitude. This effect was reversed by washout of drugs with aCSF. ***G***, Cycle-by-cycle variability estimated by Poincare plots revealed that riluzole increased short-term cycle variability. Values are shown as means ± SEM. *Indicates mean values significantly different from aCSF conditions with $p < 0.05$.

placing them 12.2 mm posterior, 2 mm either side, and 5.5 mm ventral to bregma with the guide cannulas secured in place with dental acrylic. The rat recovered for 1 week before the experiment.

On the day of the experiment, the rat was transiently anesthetized (isoflurane 2–2.5%) for the careful and accurate placement of the microdialysis probes (CX-I-12–01, Eicom) as described above for the anesthetized preparation, i.e., to ensure consistent placements within and between preparations. After placements of the microdialysis probes, the rat was connected to the recording apparatus which allowed electrophysiological signals to be recorded while the rat moved freely in a large open-topped Plexiglas bowl filled with fresh bedding, food, and water. The bowl was placed on a rotating turntable (Raturn, BASi) which automatically adjusts its position when the rat moves to avoid entanglements of the microdialysis tubing and recording cable. After a recovery period from anesthesia of at least 120 min (with the rat apparently behaving normally after ~45 min), the EEG, neck and diaphragm muscle activities were recorded during bilateral perfusion of aCSF into both preBötC and subsequent drugs. For every 10 s epoch, sleep–wake state was classified as active wakefulness, quiet wakefulness, rapid eye movement (REM), and non-REM sleep, and physiological values were calculated for every epoch. Prevailing sleep–wake states were identified according to standard criteria (Morrison et al., 2003). Briefly, EEG frequencies in the following frequency bands: δ_2 (0.5–2 Hz), δ_1 (2–4 Hz), θ (4–7.5 Hz), α (7.5–13.5 Hz), β_1 (13.5–20 Hz), and β_2 (20–30 Hz) were calculated. Active wakefulness was characterized by low δ frequencies and high neck muscle activity, whereas quiet wakefulness low δ frequencies and low neck muscle activity. Non-REM sleep was characterized by high δ frequencies, high EEG amplitude, and low neck muscle activity, whereas REM sleep presented low δ frequencies, high θ frequencies, and low neck muscle activity. Averaged baseline values were calculated over a 30 min period before blockers were microperfused. Riluzole and/or ZD7288 were then added to the perfusing solution for 240 min and average values were calculated over the last 30 min of this period. In the event that drugs did not change rhythm, DAMGO, a μ-opioid receptor agonist known to

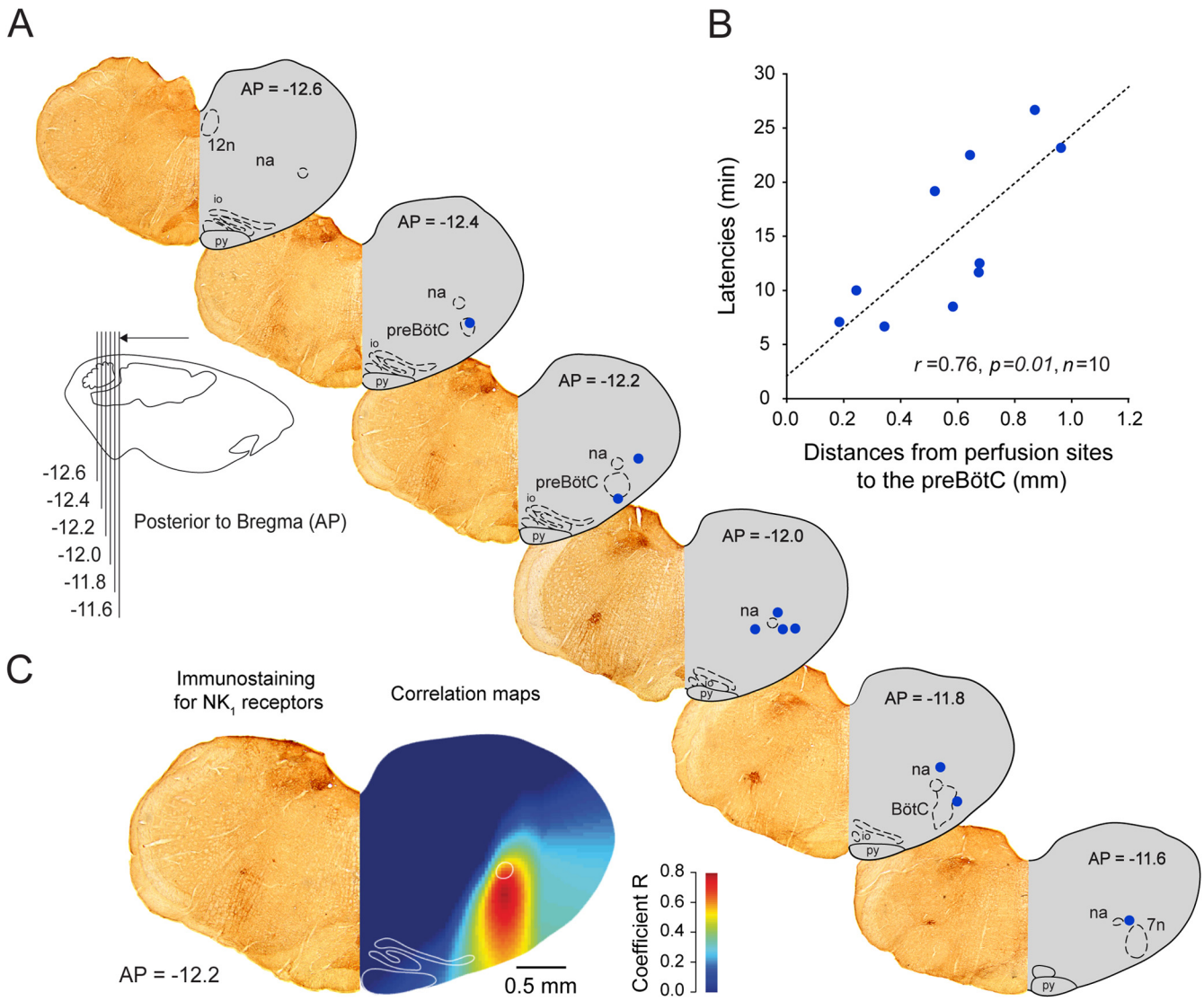

Figure 4. Anatomical sites of action of the I_{NaP} blocker riluzole and NK1R expression in the ventrolateral medulla. ***A***, Sections showing NK1R expression (left hemisection) and microperfusion sites (right hemisection, blue circles) in the ventrolateral medulla 12.6–11.6 mm posterior to bregma. The perfusion sites were in the vicinity of the preBötC. Each perfusion site corresponds to one experiment with microperfusion in the preBötC region. ***B***, There was a significant correlation between the latencies for riluzole to depress frequency by 10% and the distances of the perfusion sites from the preBötC (coordinates AP = −12.2, ML = 2.2, AP = −10.4) in anesthetized rats, showing that perfusion of drugs close to the preBötC has a faster effect on frequency than perfusion away from it. ***C***, A correlation map shows that the neural site most sensitive to riluzole corresponds to NK1R expression.

depress frequency by its action on preBötC neurons (Montandon et al., 2011), was microperfused as positive control for accurate placement of probe. Measurements started at ~11.00 and ended at ~17.00. Data were amplified, filtered, moving-time averaged, sampled, and analyzed as described previously (Montandon et al., 2011).

To determine synchronization of postural neck muscle and diaphragm muscle activities, we computed the cross-correlation function using MATLAB Signal Processing Toolbox (function *xcorr* MATLAB R12, Mathworks). This function is a measure of similarity of two waveforms. Cross-correlation function was calculated for each 10 s segment and associated with a specific state.

Two-way repeated-measure ANOVAs (sleep–wake states and drug application being the repeated factors) followed by Holm–Sidak *post hoc* tests were used to determine the state-dependent effect of manipulation of preBötC for each physiological variable. $p < 0.05$ was considered significant.

Construction of correlation maps. To determine the locations of the intervention (perfusion) sites, we cut 50 μm sections with cryostat and stained them with neutral red. Under light microscope (BX41, Olympus), we followed the track made by the microperfusion probe and identified the end of the track as the tip of the probe. To determine the anterior–posterior (AP) coordinate, we used the caudal end of the facial nucleus as the reference point (located 11.6 mm posterior to bregma) and counted the number of sections caudal to the facial nucleus until the perfusion site was reached. The dorsal-ventral (DV) and medial-lateral (ML) coordinates were then identified using the nucleus ambiguus, inferior olive, and standard brain maps (Paxinos and Watson, 1998). We constructed correlation maps to relate the location of the intervention sites with the resultant effect on respiratory activity as previously described (Montandon et al., 2011). The rationale for the construction of correlation maps is that for a locus of effect of drugs at any particular brainstem site, the latency for the drug to diffuse through the tissue and to progressively change respiratory activity will vary as a function of the distance of the probe from the effective site. We then calculated the distance from an arbitrary set of coordinates such as the preBötC to the perfusion site. We estimated the latency to a 10% change in respiratory frequency in response to ZD7288 or riluzole. Using this approach, one latency and one distance was obtained for each animal/experiment. For a specific set of experiments including many rats, we then calculated the relationship between latency of drug effects and distances from microperfusion sites to the preBötC. Each experiment in each rat contrib-

uted a single point to the correlation. This approach can also be applied to every possible set of coordinates within a 3-D grid (resolution 50 μm) spanning from 11.6 to 12.6 mm caudal to bregma. Correlation coefficients were then calculated between distances and latencies to see whether it is likely that the drugs are acting on other neural sites. Overall, this approach identifies the sites in the brainstem that respond the fastest to agent perfusion. Using MATLAB 12 software (Mathworks), correlation coefficients ($0<r^2<1$) were calculated for every set of coordinates and plotted as color pixels (blue to red) in standard brain maps. To determine the relationship between the location of microperfusion site and the latency to induce an effect on respiratory rhythm, this approach requires to use a unilateral approach where only one neural site is progressively affected by drug microperfusion. For this reason, correlation maps were only constructed for the experiments involving unilateral microperfusion.

Immunohistochemistry of neurokinin-1 receptors. We used neurokinin-1 receptor (NK1R) immunohistochemistry to locate preBötC neurons in brainstem sections (Gray et al., 2001) using techniques previously described (Montandon et al., 2011). Following fixation in 4% paraformaldehyde and cryoprotection in 30% sucrose, the brains ($n = 3$) were frozen and cut in 50 μm sections. The antibodies used were rabbit anti-NK1R (1:1000, AB-N04; Advanced Targeting Systems) and donkey anti-rabbit immunoglobin G (1:100, Jackson ImmunoResearch Laboratories). Sections were stained with a chromogen diaminobenzidine solution and were mounted on slides, dried, and sealed with Cytoseal 280. Sections spanning from 11.6 to 12.6 mm posterior to bregma were digitized with a CCD camera (Infinity 1, Olympus) and microscope (BX-41, Olympus). We then counted the number of NK1R-positive cells in a 1-mm-diameter circle placed ventral to the nucleus ambiguus on each section of the ventrolateral medulla (every 200 μm, 11.6–12.6 caudal to bregma). We then calculated the density of NK1R-positive cells as number of positive cells per mm^2 and identified the preBötC as the region with the highest density.

Results

I_h contributes to respiratory rhythm *in vivo*

To determine the contribution of I_h to the generation of respiratory rhythm *in vivo*, we locally microperfused the I_h blocker ZD7288 into the preBötC of anesthetized adult rats while recording respiratory activity. Unilateral microperfusion of ZD7288 (100 μM) into the preBötC (Fig. 1*A–C*), at concentration known to substantially block I_h *in vitro* (Gasparini and DiFrancesco, 1997; Thoby-Brisson et al., 2000), decreased respiratory frequency (f_R) by 37.7% (aCSF, f_R = 44.1 ± 3.3 breath/min; ZD7288, f_R = 28.0 ± 2.6 breath/min; $p = 0.029$, $n = 5$) (Fig. 1*C*), but did not significantly change the amplitude of diaphragm muscle activity ($p = 0.273$, $n = 5$). We used Poincare plots to quantify cycle-by-cycle variability and showed that ZD7288 increased short-term cycle variability by 180.2% compared with aCSF ($p = 0.007$) (Fig. 1*D*). Microperfusion into the preBötC of zatebradine (50 μM), another I_h blocker (Matt et al., 2011), decreased respiratory frequency by 25.8% (aCSF, f_R = 42.2 breath/min; zatebradine, f_R = 31.3 ± 0.7 breath/min; $p = 0.002$, $n = 3$) (Fig. 1*E*), replicating the effect produced by ZD7288. There also was a significant decreased in diaphragm muscle amplitude (decrease of 13.4 ± 2.1%, $p = 0.023$, $n = 3$).

To overcome the spatial limitations inherent to the localized pharmacological manipulation of selected neuronal groups in specific brain regions, we used a functional and anatomical approach to identify the sites in the medulla most sensitive to the applied agents (Montandon et al., 2011). Using the capacity of ZD7288 to diffuse through the tissue and progressively induce a reduction in respiratory frequency depending on physical proximity of the intervention site to the effective site, we related the latency for ZD7288 to decrease respiratory frequency by 10% to the proximity of the microperfusion site to the preBötC (Fig. 2*A*). Microperfusion of ZD7288 within the preBötC caused a relatively

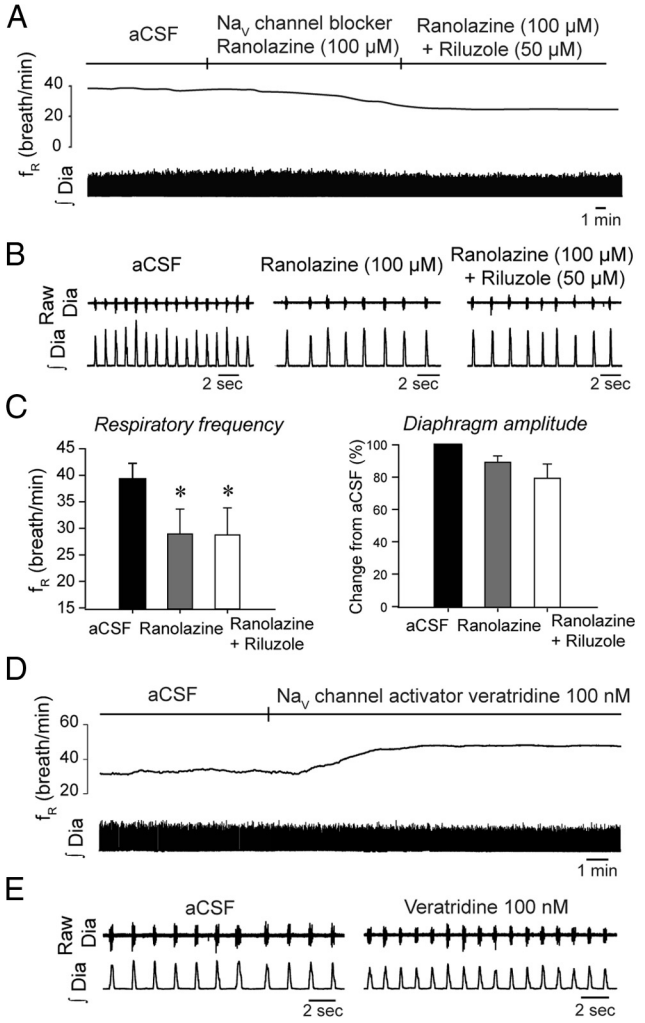

Figure 5. Blockade or activation of Na_V1 channels at the preBötC decreases or increases respiratory rhythm respectively. ***A***, ***B***, Unilateral microperfusion of the I_{NaP} blocker ranolazine into the preBötC of anesthetized rats decreased respiratory frequency, without significantly affecting diaphragm amplitude. Addition of riluzole to the perfusion medium did not decrease further respiratory frequency. ***C***, Mean data show significant changes for respiratory frequency ($n = 5$). ***D***, ***E***, Unilateral microperfusion of the I_{NaP} activator veratridine increased respiratory frequency, with no effect on diaphragm amplitude. Data representative of 4 rats. Values are shown as means ± SEM. *Indicates mean values significantly different from aCSF conditions with $p < 0.05$.

fast decrease in respiratory frequency, whereas perfusion further from the preBötC induced a slower decrease in respiratory frequency (Fig. 2*B*). There was a significant relationship between latency of response and distance from the preBötC to the perfusion sites ($r = 0.836$, $p = 0.005$, $n = 9$). For all the possible coordinates within the volume of brainstem surrounding the preBötC (see Materials and Methods), we calculated coefficients of correlation relating the latencies for respiratory slowing with distances from these coordinates to the perfusion sites (Fig. 2*C*). Construction of an anatomical map reveals "hotspot" regions that are statistically highly correlated with the latencies for respiratory slowing. The anatomical region most strongly associated with respiratory frequency slowing (illustrated in red on correlation map) corresponds to the preBötC as identified by high NK1R expression (Fig. 2*C–D*), suggesting that the sites overlapping with the preBötC are most rapidly sensitive to ZD7288. Importantly, this approach also showed that it is I_h blockade at the preBötC that elicits a significant decrease in respiratory fre-

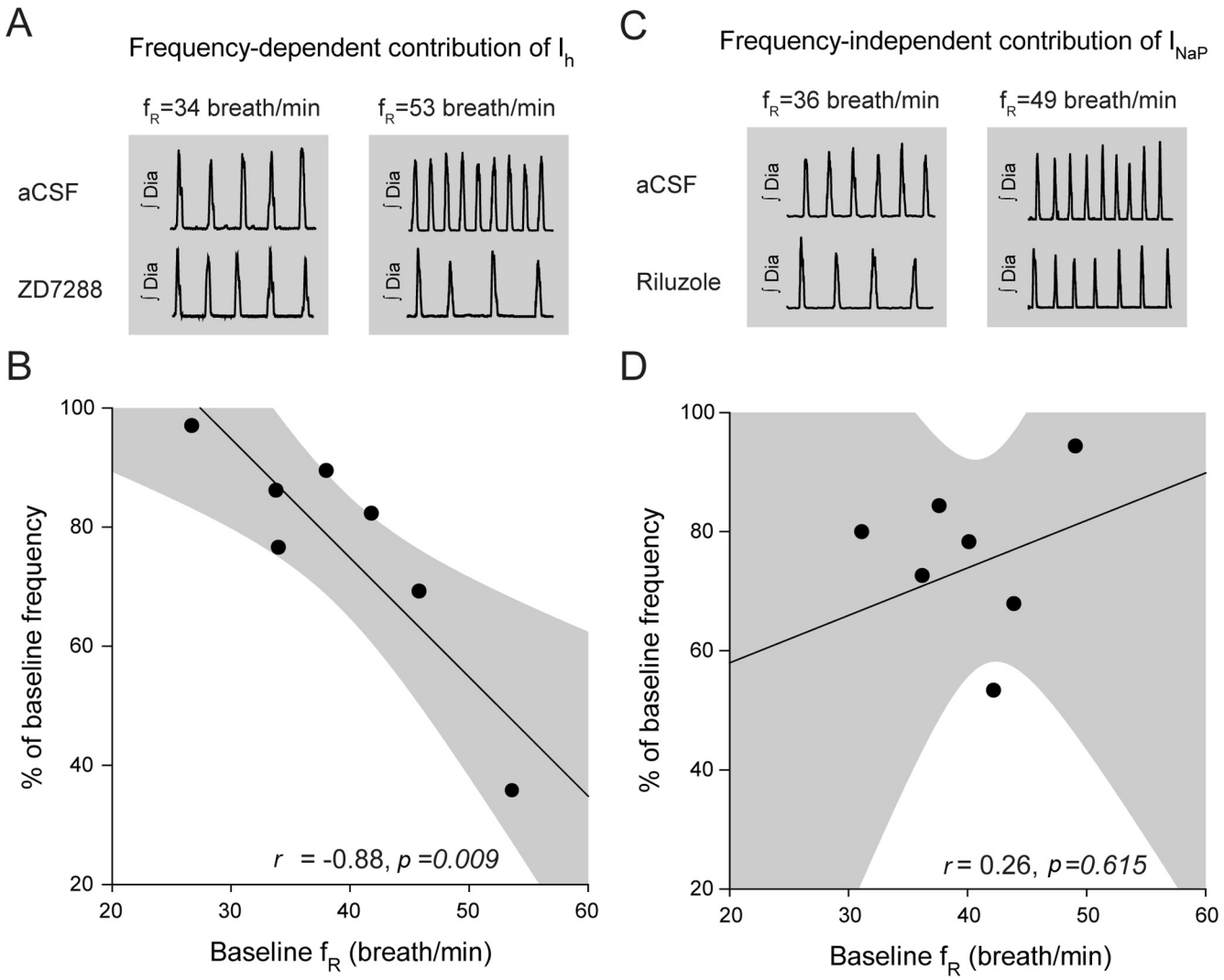

Figure 6. Frequency-dependent contribution of I_h, but not I_{NaP}, to respiratory rhythm. Relationship between baseline frequency while microperfusing aCSF into the preBötC and the changes elicited by the I_h blocker ZD7288 or the I_{NaP} blocker riluzole. ***A***, ***B***, There was a significant correlation between baseline frequency and the capacity of ZD7288 to reduce respiratory frequency (n = 7). 95% confidence interval is indicated by gray areas. ***C***, ***D***, No significant correlation was found while comparing baseline frequency and blockade by riluzole (n = 7).

quency and that effects of ZD7288 were not due to diffusion of the drug to nearby respiratory nuclei.

I_{NaP} contributes to respiratory rhythm *in vivo*

To determine the contribution of I_{NaP} to the generation of respiratory rhythm *in vivo*, we locally microperfused the I_{NaP} blocker riluzole into the preBötC of anesthetized adult rats. While recording rhythmic output from the diaphragm, riluzole was unilaterally microperfused at concentrations known to substantially block I_{NaP} *in vitro* (Del Negro et al., 2002; Pena et al., 2004). Riluzole (50 μM) into the preBötC (Fig. 3*A*) decreased respiratory frequency by 25.1% ($p = 0.025$, $n = 5$) (Fig. 3*B–D*), increased respiratory rate variability by 160.5% ($p = 0.035$, $n = 5$) (Fig. 3*E*), but did not affect diaphragm muscle amplitude ($p = 0.086$, $n = 5$) (Fig. 3*F*). Riluzole increased cycle-by-cycle short-term variability ($p = 0.033$, $n = 5$) (Fig. 3*G*). The riluzole effect on respiratory rhythm was not transient (Fig. 3*C*) as previously reported (Del Negro et al., 2005) but persisted as long as riluzole was perfused, and this effect was reversed after 45 ± 5 min of aCSF washout (Fig. 3 *B*,*D*).

Using a similar approach as with ZD7288, we related the latency for riluzole to decrease respiratory frequency by 10% to the proximity of the perfusion sites to the preBötC (Fig. 4*A*). Again there was a significant relationship between the latencies of responses and the distances of the microperfusion sites to the preBötC ($r = 0.76$, $p = 0.010$, $n = 10$) (Fig. 4*B*). A correlation map (Fig. 4*C*) showed that the anatomical region most strongly associated with slowing of respiratory frequency (illustrated in red in the correlation maps) corresponds to the preBötC as identified by NK1R expression. This result shows that the sites overlapping with preBötC are most rapidly sensitive to riluzole and that riluzole effect was not due to diffusion of the drugs to nearby respiratory nuclei, such as the medullary raphe as previously suggested (Del Negro et al., 2010).

To determine whether the observed decrease in respiratory frequency is specific to I_{NaP} blockade, we used ranolazine, another I_{NaP} blocker known to preferentially block persistent over transient sodium currents of Na_V1 channels (Kahlig et al., 2010). These channels are highly expressed in preBötC neurons (Ptak et al., 2005) and may contribute to I_{NaP} in these cells. Microperfusion of ranolazine (100 μM) into the preBötC of anesthetized adult rats decreased respiratory frequency by 25.6% ($p = 0.001$, $n = 4$) (Fig. 5*A–C*), without affecting diaphragm muscle ampli-

tude ($p = 0.103$). Subsequent addition of riluzole (50 μM) to the perfusion medium containing ranolazine did not further decrease respiratory frequency (Fig. 5*C*) suggesting that riluzole and ranolazine are blocking similar channels.

If reduction of I_{NaP} in preBötC neurons decreases respiratory frequency, then I_{NaP} activation should increase it. Accordingly, we examined the effect on the I_{NaP} activator veratridine (Fekete et al., 2009) applied to the preBötC on respiratory rhythm. Veratridine targets the neurotoxin receptor site 2 of Na_V channels and evokes a persistent sodium influx (Fekete et al., 2009). Microperfusion into the preBötC of veratridine at 100 nM, a concentration known to elicit I_{NaP} *in vitro*, increased respiratory frequency by 18.0% (aCSF, $f_R = 36.7 \pm 3.2$ breath/min; veratridine, $f_R = 43.3 \pm 3.4$ breath/min; $p = 0.039$, $n = 5$) (Fig. 5*D–E*), without affecting diaphragm amplitude ($p = 0.207$, $n = 5$).

Frequency-dependency of I_h but not I_{NaP}

One of the properties of I_h is that it can regulate oscillatory activity over a dynamic range from 0.5 to 4 Hz (Luthi and McCormick, 1998; Biel et al., 2009). This range corresponds to respiratory frequencies >30 breath/min. On the other hand, I_{NaP} can support frequencies over a broad dynamic range including lower frequencies (Koizumi and Smith, 2008). To test the frequency-dependent contribution of I_h and I_{NaP} to respiratory rhythm, we correlated the capacity of ZD7288 (100 μM) or riluzole (50 μM) to decrease respiratory frequency with the initial respiratory frequency observed in baseline conditions, i.e., in the absence of blockers. At similar levels of anesthetic, different rats exhibited various initial baseline frequencies likely due to variable sensitivities to anesthetics and/or variable placements of microperfusion probes into the preBötC region. This inherent variability provided us with a wide range of initial baseline frequencies to test the frequency-dependent contribution of I_h or I_{NaP} blockers. A significant correlation of the response to ZD7288 and the initial baseline frequency was observed ($r = -0.88$, $p = 0.009$) (Fig. 6*A*,*B*). It showed that I_h blockade has a substantial effect on reducing rhythm when it is initially high, but less so when it is low and this effect fits with the operating range of I_h. Conversely, there was no significant correlation between frequencies and I_{NaP} blockade ($r = 0.26$, $p = 0.615$) (Fig. 6*C*,*D*), showing that riluzole reduced respiratory rhythm regardless of frequency.

I_h and I_{NaP} contribute to respiratory rhythm

To determine whether I_h and I_{NaP} are essential to generate respiratory rhythm *in vivo*, we tested whether concomitant blockade of these currents would abolish respiratory activity. To first test the essential role of I_h, we perfused ZD7288 (100 μM) bilaterally into both preBötCs and observed the consequent respiratory decline in anesthetized rats. After 45 min of microperfusion, I_h blockade decreased significantly respiratory frequency by 44.0% (aCSF, $f_R = 48.7 \pm 1.5$ breath/min; bilateral ZD7288, $f_R = 24.0 \pm 7.3$ breath/min; $p = 0.049$, $n = 3$) (Fig. 7*A*) without significantly affecting the amplitude of diaphragm activity ($p = 0.184$), and did not abolished breathing within the 2 h recording period. In a separate set of experiments, we microperfused the I_h and I_{NaP} blockers into both preBötC. ZD7288 (100 μM) and riluzole (50 μM) at the preBötCs (Fig. 7*B*) substantially decreased respiratory frequency by 86.7% within 45 min (aCSF, $f_R = 43.2 \pm 3.9$ breath/min; bilateral ZD7288+riluzole, $f_R = 6.7 \pm 6.7$ breath/min, $p = 0.023$, $n = 3$) and reduced diaphragm amplitude by 75.5% ($p = 0.041$). Breathing was completely abolished after 43.3 ± 17.4 min ($n = 3$). This effect strongly differs from the effects observed with ZD7288 applied alone to both preBötCs.

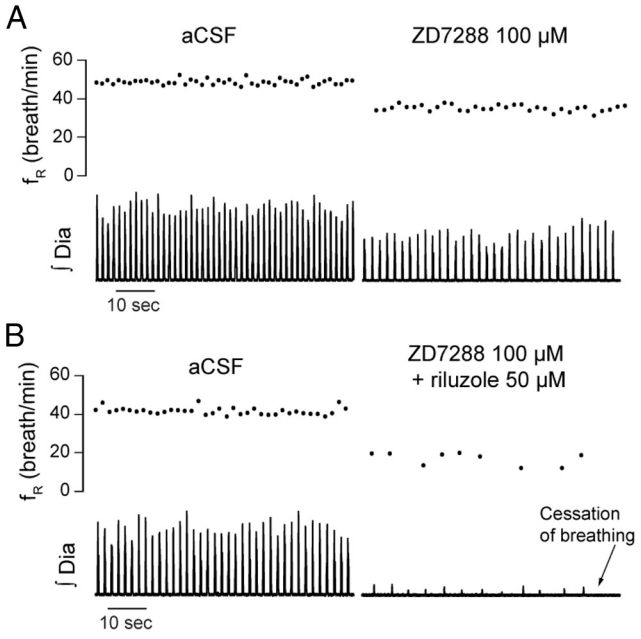

Figure 7. Bilateral blockade of I_h and I_{NaP}, but not I_h alone, abolishes respiratory rhythm. ***A***, Bilateral microperfusion of ZD7288 (100 μM) into both preBötCs decreased respiratory frequency by 44.0% ($n = 3$) after 45 min, without significantly affecting diaphragm amplitude. ***B***, Bilateral microperfusion of ZD7288 (100 μM) and riluzole (50 μM) into both preBötCs significantly decreased respiratory frequency by 86.7% and diaphragm amplitude by 75.5% within 45 min ($n = 3$). On average, breathing was abolished by ZD7288 and riluzole after 43.3 ± 17.4 min of microperfusion.

State-dependent contribution of I_h and I_{NaP} to respiratory rhythm

Respiratory rhythm is altered by anesthetics and modulated by states of arousal (Phillipson and Bowes, 1986). To determine whether I_h and I_{NaP} contribute to respiratory rhythm in the absence of anesthetics and across sleep–wake states (Fig. 8*A*), we microperfused I_h and I_{NaP} blockers into preBötCs of freely behaving and nonanesthetized adult rats as previously described (Montandon et al., 2011). Representative recordings (Fig. 8*B*,*C*) and group data (Fig. 8*D*) showed that concomitant bilateral microperfusion of ZD7288 and riluzole disrupted rhythm by decreasing respiratory frequency ($p = 0.031$, $n = 5$) (Fig. 8*B*,*C*) in quiet wakefulness (by 22.5%, $p = 0.027$), non-REM sleep (by 28.4%, $p = 0.010$), and REM sleep (by 25.7%, $p = 0.010$), but not in active wakefulness ($p = 0.720$). The respiratory pattern was also affected by I_h and I_{NaP} blockade at the preBötCs. Inspiratory durations were overall increased by the blockers across the sleep–wake cycle ($p = 0.045$) and expiratory durations were increased only in states of quiet wakefulness, non-REM, and REM sleep, but not in active wakefulness ($p < 0.001$), therefore closely following the effect observed on frequency.

Using an approach similar to the anesthesia experiments, we related the average distance from perfusion sites to preBötCs with the efficacy of the blockers to depress respiratory frequency. Two microperfusion sites were located for each experiment and the two distances from each microperfusion site to its respective preBötC were calculated and averaged. We then correlated these average distances collected in 5 experiments and the respective efficacy of blockers to decrease respiratory frequency in each ex-

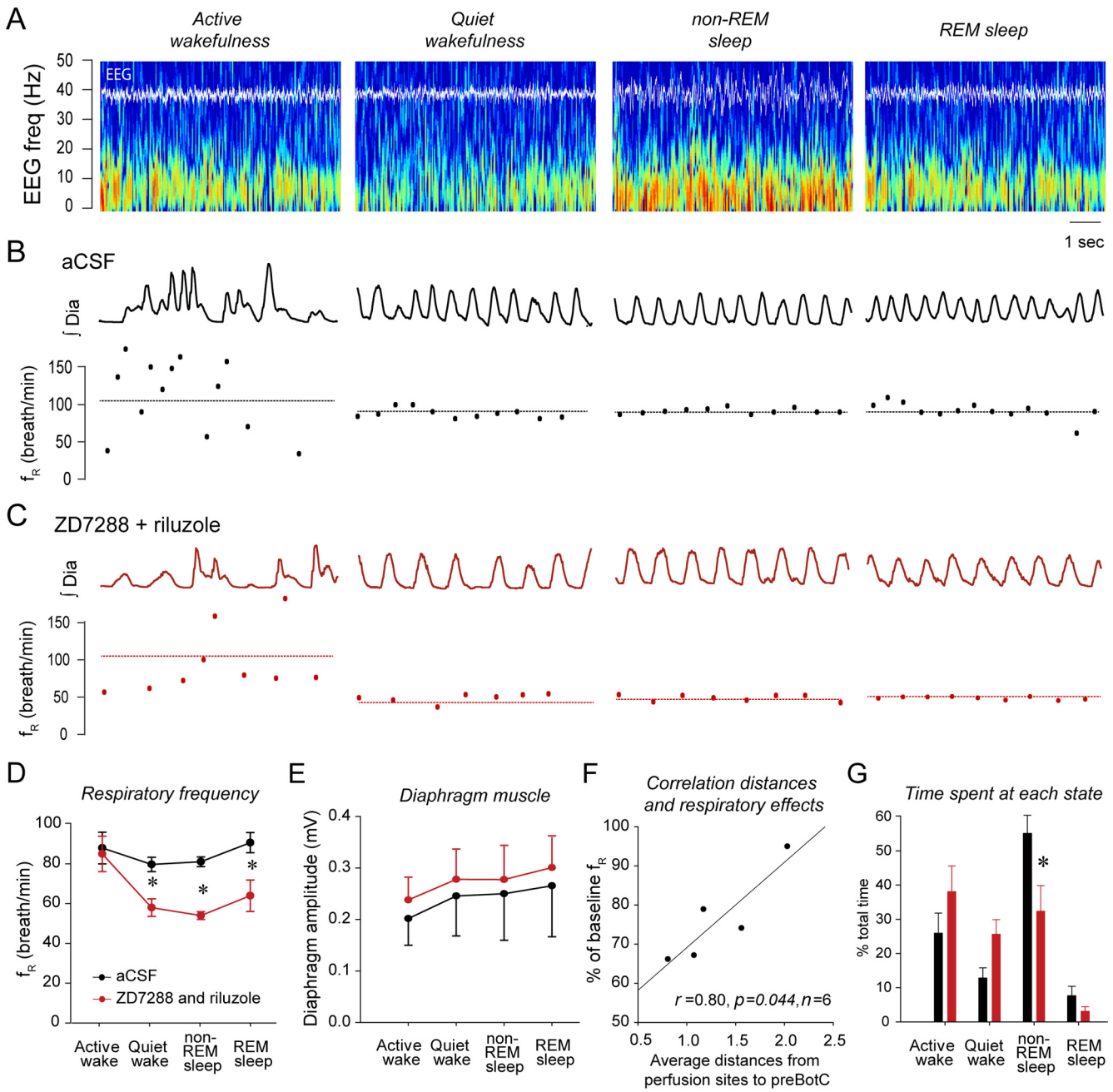

Figure 8. State-dependent contribution of I_h and I_{NaP} to respiratory rhythm. ***A***, States of active wakefulness, quiet wakefulness, non-REM and REM sleep are determined using electroencephalogram recordings and frequency spectra in freely behaving adult rats. ***B***, Diaphragm muscle recordings and cycle-by-cycle frequencies at each sleep–wake state with bilateral application at the preBötC of aCSF. ***C***, Bilateral microperfusion of ZD7288 (100 μM) and riluzole (50 μM) into both preBötCs reduced significantly respiratory frequency in states of quiet wakefulness, non-REM sleep, and REM sleep, but not in active wakefulness. ***D***, Mean data for $n = 5$ rats confirmed the state-dependent effect of drug microperfusion on respiratory frequency. ***E***, Blockade of I_h and I_{NaP} did not affect diaphragm amplitude. ***F***, Correlation of distances of perfusion sites from preBötCs and efficacy of drugs showing that close perfusion to the preBötC produced stronger effects. ***G***, Blockade of I_h and I_{NaP} and subsequent breathing reduction also reduced time spent in non-REM sleep. Values are shown as means ±SEM. *Indicates mean values significantly different from aCSF conditions with $p < 0.05$.

periment. There was a significant correlation ($r = 0.80$, $p = 0.044$, $n = 6$) (Fig. 8*F*) between average distances from microperfusion sites to preBötCs and the severity of reductions by ZD7288/riluzole suggesting that the closer the probes were to the preBötC, the stronger were the frequency reductions. Incidentally, sleep was also disrupted by perfusion of ZD7288 and riluzole into preBötCs with a reduced time spent in non-REM sleep ($p = 0.010$) (Fig. 8*G*). Bilateral microperfusion of ZD7288 (100 μM) or riluzole (50 μM) alone into the preBötC did not significantly change respiratory frequency ($p = 0.967$, $n = 5$ and $p = 0.351$, $n = 3$, respectively) (Fig. 9) across sleep–wake states.

Synchronization of respiratory and behavioral motor activities

The data described above showed that I_h and I_{NaP} at the preBötC contribute to rhythmogenesis in reduced states of brain arousal, such as sleep and anesthesia, but not in active wakefulness when the organism is engaged in complex behaviors. Active behaviors

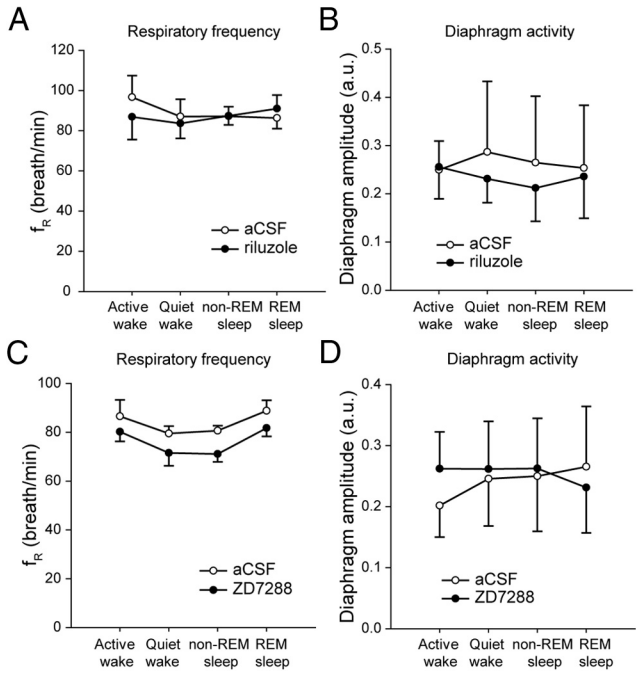

Figure 9. Blockade of I_h or I_{NaP} alone did not modify respiratory rhythm in the freely behaving adult rat. ***A***, Bilateral microperfusion of riluzole (50 μM) into the preBötC of adult rat did not affect respiratory frequency. ***B***, Diaphragm muscle activity was not modified by riluzole. ***C***, Bilateral microperfusion of ZD7288 (100 μM) at the preBötCs did not change respiratory frequency. ***D***, Diaphragm muscle amplitude was not changed by ZD7288. Values are shown as means ± SEM. *Indicates mean values significantly different from aCSF conditions with $p < 0.05$.

such as grooming or feeding are not automatic behaviors generated by the brainstem respiratory network, but rather arise from distinct cortical and cerebellar areas that impinge on the respiratory network and influence its activity to coordinate respiratory network activity to these nonrespiratory behaviors. To determine whether respiratory network activity may be modulated by other brain areas involved in distinct behaviors, we evaluated synchronization of two separate muscle activities originating from separate brain circuits. The degree of synchronization of respiratory network activity and postural motor activity was calculated using cross-correlation functions (Katz et al., 2002) between respiratory diaphragm and postural neck muscle activities. This measure shows whether two signals are synchronized independently of their intensity, which is essential to determine synchronization in signals of low amplitude such as motor activity during sleep. We showed that diaphragm muscle activity was tightly synchronized to neck muscle activity when the animal was behaviorally active or in quiet wakefulness, but not when the animal was in non-REM sleep ($p = 0.002$, $n = 3$) (Fig. 10*A*) or REM sleep ($p = 0.002$). When I_h and I_{NaP} were blocked, however, postural neck and diaphragm muscles were synchronized at all states ($p > 0.737$) (Fig. 10*B*,*C*) which differ from the state-dependent synchronization of muscle activities observed in control conditions ($p = 0.001$).

Discussion

Here, we determined the contribution of voltage-dependent inward currents in respiratory rhythmogenesis *in vivo*. We showed that I_h and I_{NaP}, two ionic currents known to mediate rhythms in many networks, mediate respiratory rhythm in states of anesthesia, quiet wakefulness, and sleep, although the network can supersede their contribution to comply its activity with active behaviors that originate from distinct neuronal circuits.

The ionic players

The unique property of I_h to activate upon hyperpolarization beyond resting potential makes it a potential current for providing rhythmicity in the respiratory network (Luthi and McCormick, 1998). When the I_h blocker ZD7288 was applied to rhythmically active brainstem sections containing the preBötC, I_h was reduced, but either no reduction of respiratory rhythm was observed (Mironov et al., 2000) or respiratory rhythm increased (Thoby-Brisson et al., 2000). This shows that I_h in preBötC neurons does not promote rhythmicity when cells are immature and isolated from the network. I_h expression is, however, reduced under these conditions, implying that its role may differ compared with mature and intact preparations (Bayliss et al., 1994; Biel et al., 2009). Here, we microperfused two distinct I_h blockers into the preBötC, at concentrations known to substantially block I_h (Williams et al., 2002; Van Bogaert and Pittoors, 2003), and we reduced respiratory rhythm. A rhythmogenic role for I_h is further evidenced by the frequency range at which it operates. I_h is involved in rhythms from 0.5 to 4 Hz (Biel et al., 2009) corresponding to respiratory frequencies between 30 and 240 breath/min. ZD7288 blocked respiratory rhythm only at frequencies >30 breath/min, consistent with I_h activation kinetics. There was also a relationship between I_h blockade and the initial baseline frequency before drug application. Frequency decline by ZD7288 was more pronounced at relatively high than low frequencies, which may explain why I_h blockers failed to depress frequency and even increased frequency in neonatal *in vitro* preparations where frequency is slow (Mironov et al., 2000; Thoby-Brisson et al., 2000). Similarly, respiratory rhythm was sensitive to NK1R blockade or to locus ceruleus stimulation only when the initial frequency was elevated (Doi and Ramirez, 2010), suggesting that distinct mechanisms mediate respiratory rhythm in low compared with high frequencies.

Surprisingly, we did not observe a significant effect of I_h blockade alone in the freely behaving experiments. The fact that I_h is activated by hyperpolarization suggests that, in strongly inhibited conditions such as anesthesia, I_h expression is increased and its physiological role is potentiated. In freely behaving animals, excitatory inputs to the preBötC may raise membrane potential above I_h activation potentials. It is, only when I_{NaP} is blocked, that I_h activation threshold would be reached. However, I_h role may be underestimated in our study. Although ZD7288 is the most potent I_h blocker currently available, it only partially blocks I_h (Gasparini and DiFrancesco, 1997). ZD7288 also inhibits T-type calcium channels (Sanchez-Alonso et al., 2008) and glutamate receptor-mediated currents (Chen, 2004), and depresses synaptic transmission (Chevaleyre and Castillo, 2002). Because these effects are only substantial when ZD7288 is applied at high concentrations for long periods, it is unlikely that ZD7288 effect was due to its action on other targets, but it cannot be excluded. Also, the fact that the I_h blocker zatebradine, which does not block calcium channels (Satoh and Yamada, 2002), also decreased respiratory rhythm, is consistent with a role of I_h in promoting respiratory rhythm. Zatebradine, however, inhibits potassium currents in some cell types (Satoh and Yamada, 2002), but such blockade would likely increase respiratory rhythm by reducing potassium outward current. Overall, our data reveal the importance of an essential ionic player in promoting respiratory rhythm in mature mammals *in vivo*, a contribution that substantially differs from its role in neonatal rodents *in vitro*.

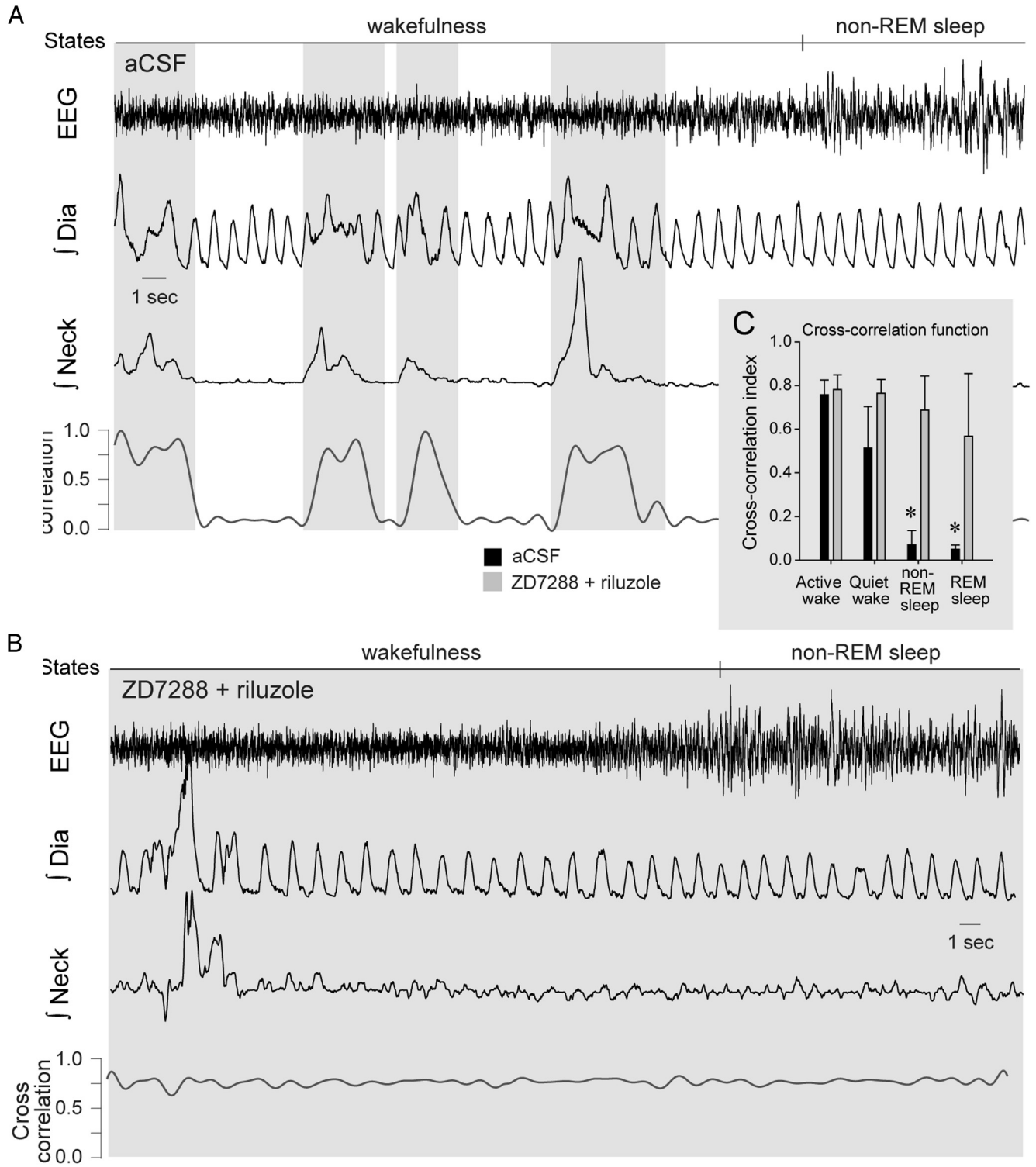

Figure 10. Synchronization of respiratory network activity and motor behavior. ***A***, Synchronization was determined by cross-correlation function of diaphragm and neck muscle activities in freely behaving adult rats. Gray areas indicate periods of synchronization; low to high synchronization corresponds to cross-correlation function from 0 to 1. ***B***, When I_h and I_{NaP} were blocked at the preBötC, high synchronization was observed across states. ***C***, Mean data show that in control conditions (aCSF, black bars), synchronization was high in active wakefulness but low in quiet wakefulness, non-REM sleep and REM sleep, whereas with I_h and I_{NaP} blockade (gray bars) synchronization occurred across states. Values are shown as means ± SEM. *Indicates mean values significantly different from aCSF conditions with $p < 0.05$.

However, I_h is not sufficient to generate respiratory rhythm by itself, because its blockade did not completely abolish rhythm. I_h interacts with other ionic currents. I_{NaP} for instance is important for rhythm generation in specific configurations of the respiratory network in hypoxia (Pena et al., 2004; Paton et al., 2006) and in neonatal rodents *in vivo* (Pena and Aguileta, 2007). Here, we show that blockade, or activation, of I_{NaP} at the preBötC, respectively decreased or increased, frequency. Correlation maps strongly suggest that riluzole is acting in the preBötC region and not in adjacent regions, such as the medullary raphe (Del Negro

et al., 2010). In addition, low concentration of riluzole avoids unspecific effects observed at higher concentrations (Urbani and Belluzzi, 2000). Voltage-gated sodium channels, which are present in high density in preBötC neurons (Ptak et al., 2005), contribute to I_{NaP} in many types of neurons (Kahlig et al., 2010). Blockade of the persistent component of sodium channels with ranolazine, or activation with veratridine, substantially suppressed or increased respiratory rhythm, respectively, supporting the contribution of I_{NaP} and its underlying channels to respiratory rhythm *in vivo*. In the freely behaving animal, riluzole did not affect respiratory rhythm which is consistent with previous data in conscious mature rats (St-John et al., 2007). In immature rodents studied *in vivo*, however, respiratory rhythm was increased after systemic administration of riluzole (Pena and Aguileta, 2007), again highlighting differences between immature and mature respiratory networks.

Concomitant blockade of I_h and I_{NaP}

During hyperpolarization, I_h induces slow membrane depolarization (Pape, 1996) which activates I_{NaP}. This mechanism has been described in the cerebellum (Williams et al., 2002), in subthreshold oscillations of the entorhinal cortex (Dickson et al., 2000), and in single-spike activity in subthalamic neurons (Beurrier et al., 2000). Consistent with this mechanism, we demonstrated that when I_h or I_{NaP} alone were blocked in the anesthetized preparation, respiratory rhythm was reduced but not abolished, and only the concomitant blockade of both currents led to rhythm cessation. I_h/I_{NaP} blockade abolishes breathing only under anesthesia, but not in freely behaving organisms, suggesting either that anesthetics are essential to abolish rhythm or that an alternative mechanism of rhythmogenesis is triggered when these currents are absent in nonanesthetized animals. Similarly, reduced ventilation due to I_h/I_{NaP} blockade likely increases carbon dioxide levels, which may stimulate rhythm, and minimize the effects of I_h/I_{NaP} blockade. Overall, these currents are necessary but probably not sufficient to generate respiratory rhythm, and the contribution of other currents cannot be excluded (Pena et al., 2004; Koch et al., 2013). In summary, under normal physiological conditions and when ionic currents and the underlying channels are fully mature, respiratory rhythmogenesis depends on a set of currents which includes I_h and I_{NaP}.

State dependency

The brain can override automatic respiratory rhythm to synchronize breathing with other behaviors (such as feeding or grooming) which also engage the respiratory system (Ramirez and Garcia, 2007). Here, we showed that I_h and I_{NaP} play key roles in respiratory rhythmogenesis, but that their contribution is overridden when the organism is behaviorally active. The locus ceruleus, a pontine structure with noradrenergic projections to the preBötC (Doi and Ramirez, 2010), is active when the organism is engaged in behaviors and is inactive in sleep (Aston-Jones and Bloom, 1981; Takahashi et al., 2010). Combined with the fact that noradrenaline directly inhibits I_h (Wang et al., 2007), high locus ceruleus activity may therefore reduce I_h expression in preBötC cells to supersede rhythm and coordinate diaphragm activity to nonrhythmic motor behaviors. When I_h and I_{NaP} are blocked, however, postural and respiratory muscles are synchronized across states, suggesting that a mechanism independent of I_h/I_{NaP} maintains respiratory rhythm. Under anesthesia, I_h/I_{NaP} blockade abolishes rhythm, and volatile anesthetics may prevent the respiratory network to recruit an alternative mechanism to sustain rhythm as observed in the freely behaving animal. The mechanism mediating synchronized activity of motor outputs is unknown and it cannot be excluded that indirect effects, such as hypercapnia may trigger their synchronization. The idea of multiple mechanisms generating rhythm within the preBötC has been proposed previously (Pena et al., 2004; Smith et al., 2009) and these state-dependent changes identify that there are multiple and redundant mechanisms that functionally cooperate to maintain respiratory rhythm, with one or other predominating as circumstances vary.

Mechanisms of rhythmogenesis

Voltage-dependent inward currents, such as I_h and I_{NaP}, are found in cells of various rhythmic networks and are essential to trigger spontaneous bursting (Pena et al., 2004; Biel et al., 2009). It is unknown, however, whether subthreshold voltage-activated inward currents contribute to spontaneous pacemaker-like bursting of mature preBötC neurons. Here, we did not record the bursting of preBötC neurons *in vivo*, but highlight I_h/I_{NaP} importance in generating respiratory rhythm in freely behaving mature organisms. Also, I_h/I_{NaP} mediate the overall excitability of the rhythmic network (Biel et al., 2009; Del Negro et al., 2010), and their blockade may decrease neuronal excitability which would decrease rhythm independently of an action on pacemaker properties. Blockade of I_{NaP} abolishes respiratory rhythm *in vitro* (Pena et al., 2004), but rhythm can be reestablished by exciting the respiratory network through AMPA or NK1Rs (Del Negro et al., 2010). Similarly, our study shows that I_h/I_{NaP} blockade and the consequent rhythm inhibition may be reactivated by excitatory inputs during active states. This is consistent with the idea that ionic conductances are important for respiratory rhythm in some conditions or states (quiet wakefulness and sleep), but are superseded by excitatory inputs when the organism is behaviorally active.

References

Aston-Jones G, Bloom FE (1981) Activity of norepinephrine-containing locus ceruleus neurons in behaving rats anticipates fluctuations in the sleep-waking cycle. J Neurosci 1:876–886. Medline

Bayliss DA, Viana F, Bellingham MC, Berger AJ (1994) Characteristics and postnatal development of a hyperpolarization-activated inward current in rat hypoglossal motoneurons in vitro. J Neurophysiol 71:119–128. Medline

Beurrier C, Bioulac B, Hammond C (2000) Slowly inactivating sodium current (I(NaP)) underlies single-spike activity in rat subthalamic neurons. J Neurophysiol 83:1951–1957. Medline

Biel M, Wahl-Schott C, Michalakis S, Zong X (2009) Hyperpolarization-activated cation channels: from genes to function. Physiol Rev 89:847–885. CrossRef Medline

Chen C (2004) ZD7288 inhibits postsynaptic glutamate receptor-mediated responses at hippocampal perforant path-granule cell synapses. Eur J Neurosci 19:643–649. CrossRef Medline

Chevaleyre V, Castillo PE (2002) Assessing the role of I_h channels in synaptic transmission and mossy fiber LTP. Proc Natl Acad Sci U S A 99:9538–9543. CrossRef Medline

Cho HJ, Furness JB, Jennings EA (2011) Postnatal maturation of the hyperpolarization-activated cation current, I_h, in trigeminal sensory neurons. J Neurophysiol 106:2045–2056. CrossRef Medline

Del Negro CA, Morgado-Valle C, Feldman JL (2002) Respiratory rhythm: an emergent network property? Neuron 34:821–830. CrossRef Medline

Del Negro CA, Morgado-Valle C, Hayes JA, Mackay DD, Pace RW, Crowder EA, Feldman JL (2005) Sodium and calcium current-mediated pacemaker neurons and respiratory rhythm generation. J Neurosci 25:446–453. CrossRef Medline

Del Negro CA, Hayes JA, Pace RW, Brush BR, Teruyama R, Feldman JL (2010) Synaptically activated burst-generating conductances may underlie a group-pacemaker mechanism for respiratory rhythm generation in mammals. Prog Brain Res 187:111–136. CrossRef Medline

Dickson CT, Magistretti J, Shalinsky MH, Fransén E, Hasselmo ME, Alonso A (2000) Properties and role of I(h) in the pacing of subthreshold oscillations in entorhinal cortex layer II neurons. J Neurophysiol 83:2562–2579. Medline

Doi A, Ramirez JM (2010) State-dependent interactions between excitatory neuromodulators in the neuronal control of breathing. J Neurosci 30: 8251–8262. CrossRef Medline

Fekete A, Franklin L, Ikemoto T, Rózsa B, Lendvai B, Sylvester Vizi E, Zelles T (2009) Mechanism of the persistent sodium current activator veratridine-evoked Ca elevation: implication for epilepsy. J Neurochem 111:745–756. CrossRef Medline

Feldman JL, Del Negro CA (2006) Looking for inspiration: new perspectives on respiratory rhythm. Nat Rev Neurosci 7:232–242. CrossRef Medline

Gasparini S, DiFrancesco D (1997) Action of the hyperpolarization-activated current (Ih) blocker ZD 7288 in hippocampal CA1 neurons. Pflugers Arch 435:99–106. CrossRef Medline

Gray PA, Janczewski WA, Mellen N, McCrimmon DR, Feldman JL (2001) Normal breathing requires preBötzinger complex neurokinin-1 receptor-expressing neurons. Nat Neurosci 4:927–930. CrossRef Medline

Kahlig KM, Lepist I, Leung K, Rajamani S, George AL (2010) Ranolazine selectively blocks persistent current evoked by epilepsy-associated NaV 1.1 mutations. Br J Pharmacol 161:1414–1426. CrossRef Medline

Katz DB, Simon SA, Nicolelis MA (2002) Taste-specific neuronal ensembles in the gustatory cortex of awake rats. J Neurosci 22:1850–1857. Medline

Koch H, Zanella S, Elsen GE, Smith L, Doi A, Garcia AJ 3rd, Wei AD, Xun R, Kirsch S, Gomez CM, Hevner RF, Ramirez JM (2013) Stable respiratory activity requires both P/Q-type and N-type voltage-gated calcium channels. J Neurosci 33:3633–3645. CrossRef Medline

Koizumi H, Smith JC (2008) Persistent Na+ and K+-dominated leak currents contribute to respiratory rhythm generation in the pre-Bötzinger complex in vitro. J Neurosci 28:1773–1785. CrossRef Medline

Lüthi A, McCormick DA (1998) H-current: properties of a neuronal and network pacemaker. Neuron 21:9–12. CrossRef Medline

Matt L, Michalakis S, Hofmann F, Hammelmann V, Ludwig A, Biel M, Kleppisch T (2011) HCN2 channels in local inhibitory interneurons constrain LTP in the hippocampal direct perforant path. Cell Mol Life Sci 68:125–137. CrossRef Medline

McKay LC, Janczewski WA, Feldman JL (2005) Sleep-disordered breathing after targeted ablation of preBötzinger complex neurons. Nat Neurosci 8:1142–1144. CrossRef Medline

Mironov SL, Langohr K, Richter DW (2000) Hyperpolarization-activated current, I_h, in inspiratory brainstem neurons and its inhibition by hypoxia. Eur J Neurosci 12:520–526. CrossRef Medline

Montandon G, Qin W, Liu H, Ren J, Greer JJ, Horner RL (2011) PreBötzinger complex neurokinin-1 receptor-expressing neurons mediate opioid-induced respiratory depression. J Neurosci 31:1292–1301. CrossRef Medline

Morrison JL, Sood S, Liu H, Park E, Liu X, Nolan P, Horner RL (2003) Role of inhibitory amino acids in control of hypoglossal motor outflow to genioglossus muscle in naturally sleeping rats. J Physiol 552:975–991. CrossRef Medline

Pape HC (1996) Queer current and pacemaker: the hyperpolarization-activated cation current in neurons. Annu Rev Physiol 58:299–327. CrossRef Medline

Paton JF, Abdala AP, Koizumi H, Smith JC, St-John WM (2006) Respiratory rhythm generation during gasping depends on persistent sodium current. Nat Neurosci 9:311–313. CrossRef Medline

Paxinos G, Watson C (1998) The rat brain in stereotaxic coordinates. San Diego: Academic.

Peña F, Aguileta MA (2007) Effects of riluzole and flufenamic acid on eupnea and gasping of neonatal mice in vivo. Neurosci Lett 415:288–293. CrossRef Medline

Peña F, Parkis MA, Tryba AK, Ramirez JM (2004) Differential contribution of pacemaker properties to the generation of respiratory rhythms during normoxia and hypoxia. Neuron 43:105–117. CrossRef Medline

Phillipson EA, Bowes G (1986) Control of breathing during sleep. In: Handbook of physiology, Section III, The respiratory system, vol. II (Cherniak NS, Widdicombe JG, eds), pp 649–989. Bethesda, MD: American Physiological Society.

Ptak K, Zummo GG, Alheid GF, Tkatch T, Surmeier DJ, McCrimmon DR (2005) Sodium currents in medullary neurons isolated from the pre-Bötzinger complex region. J Neurosci 25:5159–5170. CrossRef Medline

Ramirez JM, Garcia A 3rd (2007) Point: medullary pacemaker neurons are essential for both eupnea and gasping in mammals. J Appl Physiol 103: 717–718; discussion 722. CrossRef Medline

Sánchez-Alonso JL, Halliwell JV, Colino A (2008) ZD 7288 inhibits T-type calcium current in rat hippocampal pyramidal cells. Neurosci Lett 439: 275–280. CrossRef Medline

Satoh TO, Yamada M (2002) Multiple inhibitory effects of zatebradine (UL-FS 49) on the electrophysiological properties of retinal rod photoreceptors. Pflugers Arch 443:532–540. CrossRef Medline

Smith JC, Ellenberger HH, Ballanyi K, Richter DW, Feldman JL (1991) Pre-Bötzinger complex: a brainstem region that may generate respiratory rhythm in mammals. Science 254:726–729. CrossRef Medline

Smith JC, Abdala AP, Rybak IA, Paton JF (2009) Structural and functional architecture of respiratory networks in the mammalian brainstem. Philos Trans R Soc Lond B Biol Sci 364:2577–2587. CrossRef Medline

St-John WM, Waki H, Dutschmann M, Paton JF (2007) Maintenance of eupnea of in situ and in vivo rats following riluzole: a blocker of persistent sodium channels. Respir Physiol Neurobiol 155:97–100. CrossRef Medline

Takahashi K, Kayama Y, Lin JS, Sakai K (2010) Locus coeruleus neuronal activity during the sleep-waking cycle in mice. Neuroscience 169:1115–1126. CrossRef Medline

Thoby-Brisson M, Telgkamp P, Ramirez JM (2000) The role of the hyperpolarization-activated current in modulating rhythmic activity in the isolated respiratory network of mice. J Neurosci 20:2994–3005. Medline

Urbani A, Belluzzi O (2000) Riluzole inhibits the persistent sodium current in mammalian CNS neurons. Eur J Neurosci 12:3567–3574. CrossRef Medline

Van Bogaert PP, Pittoors F (2003) Use-dependent blockade of cardiac pacemaker current (If) by cilobradine and zatebradine. Eur J Pharmacol 478: 161–171. CrossRef Medline

Wang M, Ramos BP, Paspalas CD, Shu Y, Simen A, Duque A, Vijayraghavan S, Brennan A, Dudley A, Nou E, Mazer JA, McCormick DA, Arnsten AF (2007) Alpha2A-adrenoceptors strengthen working memory networks by inhibiting cAMP-HCN channel signaling in prefrontal cortex. Cell 129:397–410. CrossRef Medline

Williams SR, Christensen SR, Stuart GJ, Häusser M (2002) Membrane potential bistability is controlled by the hyperpolarization-activated current I(H) in rat cerebellar Purkinje neurons in vitro. J Physiol 539:469–483. CrossRef Medline

Zhong G, Masino MA, Harris-Warrick RM (2007) Persistent sodium currents participate in fictive locomotion generation in neonatal mouse spinal cord. J Neurosci 27:4507–4518. CrossRef Medline